Hydrogen Bonds

DOI: 10.1002/anie.201209273

The Nature of Hydrogen Bonding in Protic Ionic Liquids**

*Robert Hayes, Silvia Imberti, Gregory G. Warr, and Rob Atkin**

Since the days of Latimer and Rodebush,[1] much interest has been directed to understanding how liquids hydrogen (H-) bond.[2–7] Whilst H-bonds are not unique to,[8,9] or present in all liquids,[4] they are important in chemistry because H-bonds can induce solvent structure; the H-bond is a strong, directional interaction compared to other forces between liquid molecules (e.g. van der Waals, π–π, hydrophobic, or solvophobic interactions). In most liquids, H-bonding results in a preferred orientation between nearest-neighbor species, for example, dimers of formic acid.[10] However, multiple H-bonds can act cooperatively over longer distances exemplified by water's tetrahedral network structure.[1,7,11] Thus, H-bonds are key to many aspects of liquid chemistry including dynamics, solvation, and macroscopic physical properties.[4]

Here, we systematically examine how protic ionic liquids (PILs) H-bond. PILs are an emerging class of solvents composed entirely of ions.[12,13] Despite their pure ionic composition, H-bonds are a hallmark of PILs[15–18] as donor and acceptor groups are formed on the ions during synthesis via proton transfer.[14]

Whilst it is widely accepted that PILs form H-bonds,[12] its contribution to solvent (nano-)structure[19–29] and macroscopic physical properties[12,14,30–32] is difficult to deconvolute from other ion–ion interactions. Here we use model fits[33] to neutron diffraction data to examine the local arrangement of H-bonding atoms in PILs (Table 1). Unlike other techniques, neutron diffraction is sensitive to the positions of hydrogen atoms, allowing the location of hydrogens participating in H-bonds to be unambiguously determined. Strikingly, we show that H-bond direction and strength can be related to macroscopic physical properties.

The past thirty years have witnessed considerable progress towards structure–property relationships in liquids, aided in part by greater knowledge of intermolecular forces.[4] A consistent theme is that the liquid phase is not "unstructured" as it can possess time-averaged bulk structure. In scattering experiments, this is manifested as peaks in the measured structure factor $S(q)$, which corresponds to repeating inter- or intramolecular correlations in the bulk. This is shown for various primary alkylammonium salt PILs in Figures S_1–S_4 in the Supporting Information, which present $S(q)$ neutron diffraction data and the empirical potential structure refinement (EPSR)[33] model fits for EASCN, BASCN, EAHS, and EAF with multiple isotopic substitutions. We reported the diffraction spectra and fits for EAN and PAN previously.[23,24] Structures are detailed in Table 1. Notably, every PIL has nanoscale structure that can only be fitted with bicontinuous sponge-like models (see Supporting Information).

The nature of the H-bonds formed in the PILs is probed in three different ways in Figure 1. Data is presented as a distribution of: $H_N\cdots X$ distances (H-bond lengths, d_H) via partial radial pair correlation $g(r)$ functions (Figure 1 A); $N-H_N\cdots X$ angle (H-bond angles, θ) via angle probability distributions (Figure 1 B); combined 3D structure (distance + angle) via spatial density function (sdf) plots (Figures 1 C–H). Because each PIL has multiple (often chemically identical) acceptor sites, we here focus on the dominant H-bonds for each system; data for less important H-bond interactions are examined in the Supporting Information.

In Figure 1 A, the first peak in the $g(r)$ functions shows the average PIL H-bond lengths (d_H). EASCN (1.71 Å) and EAHS (1.62 Å) possess much shorter H-bonds than other PILs. The H-bond angle probability distributions (P_θ; Figure 1 B), which have been corrected for a conical[34] distribution, show that short H-bonding PILs have maxima at 180°, indicating a linear $N-H_N\cdots X$ arrangement is favored. Conversely, the long H-bonding PILs have maxima at ca. 110°, indicating bent H-bonds are preferred.

To elucidate this point it is useful to compare the fraction of linear H-bonds ($\%_{linear}$; Table 1) in each PIL, calculated by integrating the angular probability distributions in Figure 1 B between 165°–180° (note, by definition $\int_0^{180} P_\theta \, d\theta = 100\,\%$). As expected, EASCN and EAHS have the highest percentage of linear H-bonds at 53.1 % and 59.8 %, respectively. However in long H-bond liquids, less than 15 % of all H-bonds are linear, and this varies considerably with anion structures. For example, $\%_{linear}$ is much lower in EAF (7.5 %) than in EAN (12.1 %) even though both formate and nitrate are trigonal planar species with multiple oxygen H-bond acceptors. Likewise, there is no simple relationship between the fraction of linear H-bonds and cation alkyl chain length, but it does depend on ion packing factors detailed below.

The number of H-bond acceptor atoms per ammonium hydrogen $(R_{X:H_N})$, determined from converged coordination numbers, is presented in Table 2. These coordination numbers reflect the number of potential acceptor atoms within a specified radius from each H_N hydrogen, defined to include the nearest-neighbor maximum (Figure 1 A). In EASCN and EAHS, there is one acceptor atom for each ammonium

[*] R. Hayes, Assoc. Prof. R. Atkin
Discipline of Chemistry, The University of Newcastle
NSW 2308, Callaghan (Australia)
E-mail: rob.atkin@newcastle.edu.au
Dr. S. Imberti
STFC, Rutherford Appleton Laboratory, Didcot (UK)
Prof. G. G. Warr
School of Chemistry, The University of Sydney
NSW 2006 (Australia)

[**] This research was supported by an ARC Discovery Project (DP0986194), the AMRFP, and an ISIS grant (RB820100). R.H. thanks AINSE for a PGRA and Dr. Robert Burns for assistance in gas trapping.

Supporting information for this article is available on the WWW under http://dx.doi.org/10.1002/anie.201209273.

Table 1: PIL name, structure, melting point (T_m), glass transition temperature (T_g), ionic conductivity (κ), viscosity (η), hydrogen bond length (d_H), most probable hydrogen bond angle (θ_{max}), percentage of linear H-bonds ($\%_{linear}$) and Δr.[a]

PIL	Ion pair structure	H-bond donors/acceptors	T_m [°C]	T_g [°C]	κ [mS cm^{-1}]	η [cP]	d_H [Å]	θ_{max} [°]	$\%_{linear}$	Δr [Å]
ethylammonium thiocyanate (EASCN)	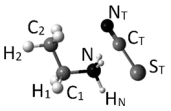	EA^+: 3 donors (H_N) SCN^-: 2 acceptors (N_T, S_T)	41	–	–	–	1.71[b]	180[c]	53.1[c]	0.99[d]
ethylammonium hydrogen sulfate (EAHS)	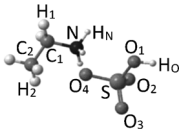	EA^+: 3 donors (H_N) HSO_4^-: 1 donor (H_O), 4 acceptors (O_1, O_2, O_3, O_4)	40	−84	4.4[e]	128	1.62[b]	180[c]	59.8[c]	0.97[d]
ethylammonium formate (EAF)	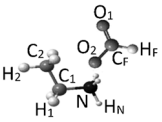	EA^+: 3 donor (H_N) HCO_2^-: 2 acceptors (O_1, O_2)	−15	−106	12.16[e]	23	2.43[b]	109[c]	7.5[c]	0.22[d]
ethylammonium nitrate (EAN)	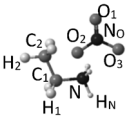	EA^+: 3 donors (H_N) NO_3^-: 3 acceptors (O_1, O_2, O_3)	12	−91.5	26.9[e]	32	2.37[b]	109[c]	12.1[c]	0.28[d]
propylammonium nitrate (PAN)	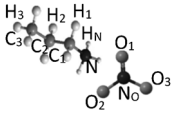	PA^+: 3 donors (H_N) NO_3^-: 3 acceptors (O_1, O_2, O_3)	3	–	12.97[f]	67	2.34[b]	112[c]	13.7[c]	0.31[d]
butylammonium thiocyanate (BASCN)	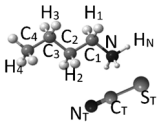	BA^+: 3 donors (H_N) SCN^-: 2 acceptors (N_T, S_T)	20.5	–	–	97	2.61[b]	106[c]	5.7[c]	0.09[d]

[a] Subscripts are used to distinguish atoms on the ions. d_H and θ_{max} determined from peaks in Figure 1 A and B, respectively. $\%_{linear} = \int_{165}^{180} P_\theta \, d\theta$ from data in Figure 1 B (note $\int_0^{180} P_\theta \, d\theta = 100$). $\Delta r = \Sigma r_{vdW} - d_H$, which is the difference between the sum of van der Waals radii of H-bonded atoms and the measured d_H. [b] Derived from data in Figure 1 A. [c] Derived from data in Figure 1 B. [d] Calculated from d_H values and data in Ref. [40]. [e] Sourced from Ref. [12]. [f] Sourced from Ref. [30].

hydrogen $(R_{X:H_N} = 1)$, and short, strong H-bonds form with 180° as the most probable bond angle.

All other PILs examined have longer H-bonds, and acceptor atoms are not close enough to each H_N atom for strong, linear H-bonds to form. Here the distribution of bond angles broadens markedly and the most probable bond angle changes from linear to ca. 110°. In these liquids, averages of $R_{X:H_N} \approx 2$ (EAN and PAN) or ≈ 3 (EAF and BASCN) acceptor atoms fall within the (larger) first coordination shell range of each hydrogen. (This need not equate to 6 or 9 acceptor atoms solvating each ammonium group, as acceptor atoms will be doubly counted if they fall within the coordination radius of two different H_N hydrogens.)

In crystalline solids, $R_{X:H_N}$ of 2 are associated with bifurcated H-bonds[3,6,8,35] and 3 with trifurcated H-bonds,[3,6,8] and similar relationships between $R_{X:H_N}$ and H-bond geometry have been reported, notably for dithiocyanate salts,[36] or thiocyanate,[37,38] and sulfate[39] anions in the Cambridge Structural Database. The bifurcated and trifurcated definitions must be applied with caution for PILs because the ions are in motion rather than fixed in a lattice, so the $R_{X:H_N}$ and angle distributions represent the average liquid state. Nonetheless, the similarity of correlations between the d_H, θ, and $R_{X:H_N}$ data for these PILs and the crystalline solids is striking, making it likely that bifurcated and trifurcated H-bonds are present in these solvents, although they may not be long lived.

These H-bonding structures are represented in Figures 1 C–H using sdf plots, which depict the most probable 3D distribution of H-bond acceptor atoms around the donor group. The radial cut-offs in the sdf plots capture all possible d_H represented up to the first local minima in the $g(r)$ data (Figure 1 A). A low 20% probability surface was used as it highlights the most favored H-bonding arrangement.

EASCN (Figure 1 C) and EAHS (Figure 1 D) have three small symmetric acceptor lobes, slightly above the plane of the NH_3^+ group, each collinear to the N–H_N covalent bonds. This is the origin of the strong H-bonding in these systems; the acceptor atoms are arranged around NH_3^+ in a 1:1 ratio that maximizes linear H-bonding interactions.

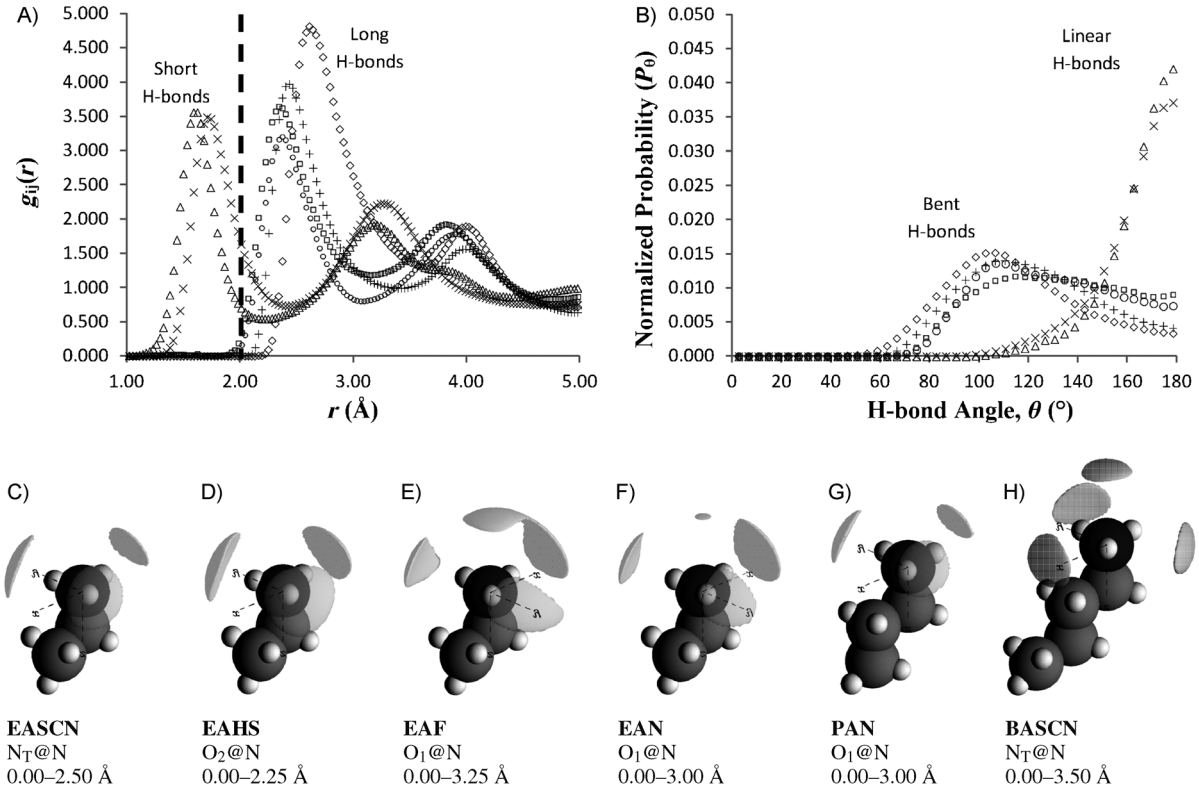

Figure 1. EASCN (×), EAHS (△), EAF (+), EAN (○) PAN (□), and BASCN (◇). A) H-bond distances: partial radial H_N···X $g(r)$ data. B) H-bond angles: normalized angle probability distribution (P_θ) of N-H_N···X triplet for all H-bond lengths up to the first local minimum in the $g(r)$ data in (A). C–H) H-bond distance + angle: sdf plots of H-bond acceptor location as a function of distance and angular position from the H-bond donor (ammonium nitrogen). The sdf data is a combined 3D representation of (A) and (B) with 20% probability surfaces shown.

Table 2: PIL H-bond classification by ion packing factors.[a]

PIL	Atom–atom $g(r)$	Coord. number (α–β)	$R_{X:H_N}$	H-bond classification
EASCN	H_N–N_T	0.55 (0–2.50)	1.01	simple
	H_N–S_T	0.46 (0–2.50)		
EAHS	H_N–O_1	0.05 (0–2.25)	1.02	simple
	H_N–O_2	0.34 (0–2.25)		
	H_N–O_3	0.32 (0–2.25)		
	H_N–O_4	0.31 (0–2.25)		
EAN	H_N–O_1	0.56 (0–3.00)	1.63	bifurcated
	H_N–O_2	0.55 (0–3.00)		
	H_N–O_3	0.52 (0–3.00)		
PAN	H_N–O_1	0.68 (0–3.00)	2.10	bifurcated
	H_N–O_2	0.72 (0–3.00)		
	H_N–O_3	0.70 (0–3.00)		
EAF	H_N–O_1	1.35 (0–3.25)	2.67	bi/trifurcated
	H_N–O_2	1.32 (0–3.25)		
BASCN	H_N–N_T	1.57 (0–3.50)	3.10	trifurcated
	H_N–S_T	1.53 (0–3.50)		

[a] Atom coordination numbers show number of acceptor atoms X around a H_N proton between limits α and β. $R_{X:H_N}$ is the ratio of total number of acceptor sites for each H_N donor site. The error in each coordination number is about ±0.05.

Other PILs have markedly different sdf plots, reflecting differences in d_H, θ, and $R_{H_N:X}$. In EAN and PAN (Figures 1F and G), three acceptor lobes are still present, but they are larger, more asymmetric, and the majority of density is off the N–H_N bond axis. This is consistent with EAN and PAN having a large proportion of bent H-bonds.

EAF and BASCN (Figures 1E and H) also have asymmetric acceptor lobes, as well as additional density directly above the NH_3^+ group. For both of these PILs, the lobes roughly bisect the H_N-N-H_N angles, and bent H-bonds are favored. Because the lobes above the NH_3^+ group form acute angles to the N–H_N donors, it is likely that this corresponds to anions electrostatically attracted to the cation, rather than conventionally H-bonded.

As the cation and anion in each system form more than one H-bond, all PILs build up dense, cooperative H-bond networks in the bicontinuous nanostructure. The relative H-bond strengths in these networks can be determined from Δr values (Table 1), which is the difference between sum of the van der Waals radii[40] of the H-bond donor-acceptor triplet (Σr_{vdW}) and the measured d_H. Whilst the van der Waals definition of H-bonds is outdated,[8] Δr is known to be proportional to H-bond strength,[41] and is about three times larger for EASCN and EAHS than other PILs.

Differences in H-bonding are reflected in macroscopic physical properties (Table 1), particularly for PILs with

a common ion. The strong, linear H-bonding PILs have more "solid-like" character, whereas weaker, bent H-bonding systems display more "liquid-like" properties. For example, T_m and T_g are known to increase with cohesive interactions; in ethylammonium PILs, the trend in T_m and T_g is the same as that for H-bond strength, i.e., EASCN > EAHS > EAN > EAF. Table 1 also shows a strong correlation with properties linked to ion mobility; η increases and κ decreases as H-bonding is enhanced (and vice versa), except for EAF. However, EAF is difficult to dry and is known to thermally degrade,[12,14] either of which could contribute to lower than expected conductivity.

The ion arrangements in PILs are a consequence of the balance between intermolecular forces and the physical dimensions of the ions. Whilst similar bicontinuous sponge-like nanostructures form in all systems, there is significant variation in the nature of H-bonds in present. This means that that PIL nanostructure controls the H-bond strength and structure by dictating the relative orientations of the cations and anions to each other; the distribution of H-bond geometries is related to the ability of each PIL to accommodate H-bonds in the bicontinuous arrangement rather than inducing a different bulk structure. When the nanostructure is such that a relatively high proportion of H-bonds are linear $(R_{X:H_N} \approx 1)$, attractions between ions increase and physical properties become more solid-like. At higher $R_{X:H_N}$ ratios, bifurcated or trifurcated H-bonding results, producing weaker, bent H-bonds, decreasing cation–anion attractions and leading to a more fluid-like material.

Experimental Section

EAN, EAF, EAHS, and PAN were synthesized by acid–base neutralization from appropriate concentrated reagents.[23] EASCN and BASCN were prepared according to the method described by Poole et al.[42] Chemically identical, but isotopically different contrasts for each PIL were made by selectively replacing hydrogen with deuterium on the exchangeable ($[D_3]$ or $[D_4]$ contrasts) or exchangeable and non-exchangeable ($[D_8]$ or $[D_9]$ contrasts) groups.[23]

Neutron diffraction data were collected on the SANDALS diffractometer (Rutherford Appleton Laboratories, UK) and $S(q)$ extracted as detailed in Ref. [23]. Empirical Potential Structure Refinement (EPSR)[33] was used to model the PILs. This models the bulk structure of 500 ion pairs by a standard, iterative Monte Carlo framework that is refined against the measured SANDALS data as well as other liquid parameters (see Supporting Information).

Received: November 20, 2012
Revised: January 16, 2013
Published online: February 28, 2013

Keywords: hydrogen bonds · ionic liquids · nanostructure · neutron diffration · self-assembly

[1] W. M. Latimer, W. H. Rodebush, *J. Am. Chem. Soc.* **1920**, *42*, 1419.
[2] L. Pauling, *The Nature of the Chemical Bond*, Cornell University Press, Ithaca, **1960**.
[3] G. A. Jeffrey, *An Introduction to Hydrogen Bonding*, Oxford University Press, New York, **1997**.
[4] C. Reichardt, T. Welton, *Solvents and Solvent Effects in Organic Chemistry*, 4th ed., Wiley-VCH, Weinheim, **2011**.
[5] G. Gilli, P. Gilli, *The Nature of the Hydrogen Bond: Outline of a Comprehensive Hydrogen Bond Theory*, Oxford University Press, Oxford, **2009**.
[6] G. R. Desiraju, T. Steiner, *The Weak Hydrogen Bond: In Structural Chemistry and Biology*, Oxford University Press, Oxford, **2001**.
[7] Y. Marechal, *The Hydrogen Bond and the Water Molecule*, Elsevier, Amsterdam, **2007**.
[8] T. Steiner, *Angew. Chem.* **2002**, *114*, 50; *Angew. Chem. Int. Ed.* **2002**, *41*, 48.
[9] A. C. Legon, *Chem. Soc. Rev.* **1993**, *22*, 153.
[10] S. Imberti, D. T. Bowron, *J. Phys. Condens. Matter* **2010**, *22*, 404212.
[11] A. K. Soper, *Chem. Phys.* **2000**, *258*, 121.
[12] T. L. Greaves, C. J. Drummond, *Chem. Rev.* **2008**, *108*, 206.
[13] R. Hayes, G. G. Warr, R. Atkin, *Phys. Chem. Chem. Phys.* **2010**, *12*, 1709.
[14] M. Yoshizawa, W. Xu, C. A. Angell, *J. Am. Chem. Soc.* **2003**, *125*, 15411.
[15] K. Fumino, A. Wulf, R. Ludwig, *Angew. Chem.* **2009**, *121*, 3230; *Angew. Chem. Int. Ed.* **2009**, *48*, 3184.
[16] K. Fumino, A. Wulf, R. Ludwig, *Phys. Chem. Chem. Phys.* **2009**, *11*, 8790.
[17] C. Roth, T. Peppel, K. Fumino, M. Köckerling, R. Ludwig, *Angew. Chem.* **2010**, *122*, 10419; *Angew. Chem. Int. Ed.* **2010**, *49*, 10221.
[18] K. Fumino, E. Reichert, K. Wittler, R. Hempelmann, R. Ludwig, *Angew. Chem.* **2012**, *124*, 6340; *Angew. Chem. Int. Ed.* **2012**, *51*, 6236.
[19] R. Hayes, N. Borisenko, B. Corr, G. B. Webber, F. Endres, R. Atkin, *Chem. Commun.* **2012**, *48*, 10246.
[20] R. Atkin, G. G. Warr, *J. Phys. Chem. B* **2008**, *112*, 4164.
[21] Y. Umebayashi, W. Chung, T. Mitsugi, S. Fukuda, M. Takeuchi, K. Fujii, T. Takamuku, R. Kanzaki, S. Ishiguro, *J. Comput. Chem. Jpn.* **2008**, *7*, 125.
[22] T. L. Greaves, D. F. Kennedy, S. T. Mudie, C. J. Drummond, *J. Phys. Chem. B* **2010**, *114*, 10022.
[23] R. Hayes, S. Imberti, G. G. Warr, R. Atkin, *Phys. Chem. Chem. Phys.* **2011**, *13*, 3237.
[24] R. Hayes, S. Imberti, G. G. Warr, R. Atkin, *Phys. Chem. Chem. Phys.* **2011**, *13*, 13544.
[25] R. Hayes, S. Imberti, G. G. Warr, R. Atkin, *Angew. Chem.* **2012**, *124*, 7586; *Angew. Chem. Int. Ed.* **2012**, *51*, 7468.
[26] R. Hayes, D. Wakeham, R. Atkin in *Ionic Liquids UnCOILed: Critical Expert Overviews* (Eds.: K. R. Seddon, N. Plechkova), Wiley, Hoboken, **2012**.
[27] J. Sweeney, F. Hausen, R. Hayes, G. B. Webber, F. Endres, M. W. Rutland, R. Bennewitz, R. Atkin, *Phys. Rev. Lett.* **2012**, *109*, 155502.
[28] X. Song, H. Hamano, B. Minofar, R. Kanzaki, K. Fujii, Y. Kameda, S. Kohara, M. Watanabe, S. Ishiguro, Y. Umebayashi, *J. Phys. Chem. B* **2012**, *116*, 2801.
[29] T. L. Greaves, D. F. Kennedy, A. Weerawardena, N. M. K. Tse, N. Kirby, C. J. Drummond, *J. Phys. Chem. B* **2011**, *115*, 2055.
[30] S. Bouzon Capelo, T. Mendez-Morales, J. Carrete, E. Lopez Lago, J. Vila, O. Cabeza, J. R. Rodriguez, M. Turmine, L. M. Varela, *J. Phys. Chem. B* **2012**, *116*, 11302.
[31] R. Atkin, S. M. C. Bobillier, G. G. Warr, *J. Phys. Chem. B* **2010**, *114*, 1350.
[32] J. A. Smith, O. Werzer, G. B. Webber, G. G. Warr, R. Atkin, *J. Phys. Chem. Lett.* **2010**, *1*, 64.
[33] A. K. Soper, *Phys. Rev. B* **2005**, *72*, 104204.
[34] J. Kroon, J. A. Kanters, *Nature* **1974**, *248*, 667.
[35] I. Rozas, I. Alkorta, J. Elguero, *J. Phys. Chem. A* **1998**, *102*, 9925.

[36] D. J. Wolstenholme, J. J. Weigand, E. M. Cameron, T. S. Cameron, *Cryst. Growth Des.* **2009**, *9*, 282.
[37] J. P. M. Lommerse, J. C. Cole, *Acta Crystallogr. Sect. B* **1998**, *54*, 316.
[38] L. Tchertanov, C. Pascard, *Acta Crystallogr. Sect. B* **1996**, *52*, 685.
[39] L. Chertanova, C. Pascard, *Acta Crystallogr. Sect. B* **1996**, *52*, 677.
[40] R. S. Rowland, R. Taylor, *J. Phys. Chem.* **1996**, *100*, 7384.
[41] S. J. Grabowski, *J. Phys. Chem. A* **2001**, *105*, 10739.
[42] M. E. Coddens, K. G. Furton, C. F. Poole, *J. Chromatogr.* **1986**, *356*, 59.

